Distinct ribosome maturation defects in yeast models of Diamond-Blackfan anemia and Shwachman-Diamond syndrome

Joseph B. Moore IV,[1] Jason E. Farrar,[2] Robert J. Arceci,[2] Johnson M. Liu,[3] and Steven R. Ellis[1]

[1]Department of Biochemistry and Molecular Biology, University of Louisville, Louisville; [2]Division of Pediatric Oncology, Kimmel Comprehensive Cancer Center, The Johns Hopkins University School of Medicine, Baltimore, MD, and [3]The Feinstein Institute for Medical Research, Manhasset, Schneider Children's Hospital, NY, USA

Funding: this work was supported by a grant from the National Institutes of Health (R01HL79583) to S.R.E. and the Shwachman Diamond Project to J.B.M IV and in part by grants from the Children's Cancer Foundation (RJA), the Lyles Parachini Fund (RJA), the Michael Corb Fund (RJA), the Michael Garil Leukemia Survivors Program (RJA), Alex's Lemonade Stand Foundation (JEF), the King Fahd Chair in Pediatric Oncology (RJA) and CA120535 (RJA).

Manuscript received on June 9, 2009. Revised version arrived on July 6, 2009. Manuscript accepted on July 8, 2009.

Correspondence:
Steven R. Ellis,
Department of Biochemistry and Molecular Biology,
University of Louisville,
Louisville, Kentucky
40292 USA.
E-mail: srellis@louisville.edu

ABSTRACT

Background
Diamond-Blackfan anemia and Shwachman-Diamond syndrome are inherited bone marrow failure syndromes linked to defects in ribosome synthesis. The purpose of this study was to determine whether yeast models for Diamond-Blackfan anemia and Shwachman-Diamond syndrome differed in the mechanism by which ribosome synthesis was affected.

Design and Methods
Northern blotting, pulse-chase analysis, and polysome profiling were used to study ribosome synthesis in yeast models. Localization of 60S ribosomal subunits was assessed using RPL25eGFP.

Results
Relative to wild-type controls, each disease model showed defects in 60S subunit maturation, but with distinct underlying mechanisms. In the model of Diamond-Blackfan anemia, 60S subunit maturation was disrupted at a relatively early stage with abortive complexes subject to rapid degradation. 5S ribosomal RNA, unlike other large subunit ribosomal RNA in this model, accumulated as an extra-ribosomal species. In contrast, subunit maturation in the Shwachman-Diamond syndrome model was affected at a later step, giving rise to relatively stable pre-60S particles with associated 5S ribosomal RNA retained in the nucleus.

Conclusions
These differences between the yeast Diamond-Blackfan anemia and Shwachman-Diamond syndrome models have implications for signaling mechanisms linking abortive ribosome assembly to cell fate decisions and may contribute to the divergent clinical presentations of Diamond-Blackfan anemia and Shwachman-Diamond syndrome.

Key words: bone marrow failure syndrome, abortive ribosome assembly, signaling pathways, half-mer polysomes.

Citation: Moore IV JB, Farrar JE, Arceci RJ, Liu JM, and Ellis SR. Distinct ribosome maturation defects in yeast models of Diamond-Blackfan anemia and Shwachman-Diamond syndrome. Haematologica. 2010; 95:57-64. doi:10.3324/haematol.2009.012450

©2010 Ferrata Storti Foundation. This is an open-access paper.

Introduction

Diamond-Blackfan anemia (DBA) and Shwachman-Diamond syndrome (SDS) are congenital bone marrow failure syndromes linked to defects in ribosome synthesis and/or function.[1] DBA and SDS are also characterized by a heterogeneous collection of congenital anomalies and a predisposition to cancer. Although both diseases share these general features, there are substantial differences in their clinical manifestations. DBA is characterized by a red blood cell hypoplasia, whereas SDS is frequently characterized by neutropenia, although other hematopoietic lineages may also be affected in both disorders. Patients with SDS also display exocrine pancreatic deficiency, which is not observed in DBA.[2] The congenital anomalies in SDS include short stature, skeletal defects and neurological problems. Patients with DBA also have short stature, but in contrast to SDS, craniofacial anomalies are the most commonly associated congenital malformations along with other abnormalities, including triphalangeal thumbs and genitourinary tract and cardiac defects.[3,4] Both diseases carry an increased risk of cancer, but differ in neoplastic potential and associated types of malignancies. Approximately 30-40% of SDS patients progress to develop myelodysplastic syndrome and/or acute myelogenous leukemia. The incidence of cancer in DBA patients is lower, being approximately 2%. Both solid tumors and blood-based cancers have been observed in patients with DBA.[4]

The molecular underpinnings of both DBA and SDS converge on a common target, the ribosome. To date, the genes involved in DBA all encode structural components of the ribosome. Three of these genes, *RPS17*, *RPS19* and *RPS24* encode ribosomal proteins of the 40S subunit.[5-7] More recently, *RPL5*, *RPL11*, and *RPL35A* genes encoding 60S subunit ribosomal proteins have been shown to harbor pathogenic mutations in DBA.[8,9] Several studies have shown that ribosomal proteins affected in DBA are required for the maturation of ribosomal subunits indicating that the basis for the clinical features of DBA resides in abortive ribosome synthesis.[8-12] In SDS, the gene affected is *SBDS*, which encodes a protein associated with 60S ribosomal subunits.[13] SBDS is not a structural component of the ribosome. The yeast ortholog of SBDS, Sdo1, has been reported to be required for the biogenesis and function of the 60S ribosomal subunit.[14] In contrast, there have been conflicting reports regarding the role of SBDS in the biogenesis of 60S ribosomal subunits in mammalian cells.[13] While these data indicate that both DBA and SDS may arise through defects in ribosome synthesis and/or function, little is known about how these changes in this common target result in the distinct clinical presentations of the two diseases.

Studies in animal models of DBA have recently shown that the tumor suppressor p53 plays an important role in developmental and hematologic phenotypes.[15-17] These findings are generally interpreted in the context of a model in which some form of nucleolar stress signaling promotes p53 stabilization and activation.[18] Two pathways appear ideally suited to signal features of abortive ribosome assembly to growth control and apoptosis. Both involve MDM2, a zinc-finger ubiquitin ligase, which targets p53 for proteasomal degradation. Several ribosomal proteins have now been shown to bind to MDM2 and inhibit its ubiquitin ligase activity resulting in p53 stabilization and activation.[19] In this model, ribosomal proteins are liberated from productive assembly into ribosomal subunits and are free for signaling through MDM2. Alternatively, nucleolar stress can also signal through the ARF tumor suppressor.[20] This latter pathway appears to involve nucleophosmin, a nucleolar protein recently shown to be involved in ribosome trafficking from the nucleus to the cytoplasm.[21]

The recent discoveries of genes encoding 60S subunit ribosomal proteins mutated in DBA has allowed us to focus on the large ribosomal subunit as a common target in yeast models for DBA and SDS.[8,9] These models employed yeast strains mutated in *RPL33A*, the yeast ortholog of *RPL35A* mutated in DBA,[8] and *SDO1*, the ortholog of *SBDS* mutated in SDS.[22] Our goal was to determine whether there are molecular features that differentiate the two disease models. Here we show that both models affect the production of 60S subunits, but do so by distinct mechanisms which affect different stages of the subunit maturation pathway. The subunit deficit in the DBA model is linked to an assembly defect that results in immature particles that are rapidly degraded. This assembly defect is associated with a substantial increase in the amount of extra-ribosomal 5S ribosomal RNA (rRNA). This observation is intriguing in light of the observation that, in mammalian cells, ribosomal proteins Rpl5 and Rpl11, in complex with 5S rRNA, interact with MDM2 and promote p53 stabilization and activation.[23] In contrast to the data obtained for the DBA model, the subunit deficit in the SDS model is linked to defects later in the subunit maturation pathway. As a consequence of this rather late maturation defect a significant fraction of the 60S subunit precursors found in the SDS model are retained within the nucleoplasm associated with 5S rRNA. Thus, the two disease models differ dramatically in terms of their effects on subunit assembly and the potential for subsequent diversion of ribosomal components from their normal assembly pathway to potential interactions with other growth regulatory factors within cells. These models, therefore, provide a mechanistic basis for how differing effects on 60S subunit maturation could potentially trigger alternative signaling pathways within cells that give rise to the distinct clinical phenotypes of DBA and SDS.

Design and Methods

Yeast strains

The yeast strains used in this study were generated by the Saccharomyces genome deletion project and were either obtained from Research Genetics or Euroscarf. Heterozygous diploids for *SDO1* (20519D: MAT a/α *ura3-1/ura3-1, his3-11/his3-11, leu2-3_112/leu2-3_112, trp1Δ2/trp1Δ2, ade2-1/ade2-1, can1-100/can1-100, sdo1::kanMX4/SDO1*) and *RPL33A* (*22109: MAT a/α his3Δ1/his3Δ1, leu2Δ0/leu2Δ0, lys2Δ0/+, met15Δ0/+, ura3Δ0/ura3Δ0, rpl33A::kanMX4/RPL33A*) were sporulated and resulting haploid strains were employed. Because the genetic background of the *SDO1* mutant was W303 and the *RPL33A* strain was BY4743, the *RPL33A* disruption was backcrossed into the W303 background for the experiments reported

here. The genotype of the *RPL33A* strain used was MAT *a/α ura3-1/ura3-1, his3-11/his3-11, leu2-3_112/leu2-3_112, trp1Δ2/trp1Δ2, ade2-1/ade2-1, can1-100/can1-100, rpl33A::kanMX4/RPL33A*. Because of a high spontaneous suppression rate of both *SDO1* and *RPL33A* mutants, haploid strains were freshly derived for each experiment.

Polysome profiling, northern hybridization, and pulse-chase analyses

Cell extracts were prepared for polysome analysis as outlined previously,[24] and centrifuged at 28,000 rpm for 6 h in an SW28.1 rotor (Beckman Instruments, Inc., Fullerton, CA, USA). Sucrose gradients were fractionated and the absorbance at 254 nm monitored using an ISCO model 185 gradient fractionator (Teledyne Isco, Inc., Lincoln, NE, USA) interfaced to a UA-6 absorbance detector. RNA was recovered from sucrose gradient fractions after precipitation with 2 volumes of absolute ethanol. Precipitates were collected by centrifugation for 10 min at 10,000xg and then suspended in 0.3 mL of 20 mM Tris-HCl pH 7.4, 2.5 mM EDTA, 100 mM NaCl, and 1% sodium dodecyl sulfate. Suspensions were extracted twice with phenol/chloroform and RNA in the aqueous phase was precipitated overnight at –20°C with 2.5 volumes of ethanol. RNA was washed once with 70% ethanol, dried *in vacuo*, and suspended in DEPC-treated water. RNA was fractionated on 1.5% formaldehyde-agarose gels, transferred to zeta-probe, and hybridized with oligonucleotides labeled at their 5' ends with ^{32}[P]. Oligonucleotides were radio-labeled using polynucleotide kinase and γ-^{32}[P]-ATP. The oligonucleotides employed were: 5S rRNA probe 5'-CAGTTGATCGGACGGGAACA-3', 5.8S rRNA probe 5'-CGTATCGCATTTCGCTGCGTTC-3', and C_2-ITS2 probe 5'-GGCCAGCAATTTCAAGTTA-3'. The procedures for pulse-chase analysis are described elsewhere.[24] Data were scanned and digitized using Adobe Photoshop.

Live cell fluorescence imaging

Yeast strains were transformed with PRS316-RPL25eGFP (URA3) and pUN100-DsRed-NOP1 (LEU2) vectors using an Alkali-Cation™ Yeast Kit (Qbiogene, Inc., Carlsbad, CA, USA) as directed by the manufacturer. Isolated transformants were grown to mid-log phase in synthetic complete liquid media lacking leucine and uracil. One milliliter aliquots were then taken and centrifuged at 10,000 rpm for 15 s to pellet the cells. The supernatant was discarded and the resulting pellet was washed with 0.5 mL of KPO_4/sorbitol wash solution (1.2M sorbitol, 0.1M potassium phosphate, pH 7.5). Cell pellets were then resuspended in 300 µL of KPO_4/sorbitol wash solution and 1 µL of 10 µg/mL 4',6-diamidino-2-phenylindole (DAPI) nuclear stain was added. Cell/DAPI suspensions were incubated at room temperature for 10 min. Following this incubation period, cells were washed twice with KPO4/sorbitol solution, re-suspended in 200 µL of KPO_4/sorbitol, and 2.5 µL of this cell suspension added to glass microscope slides. Cells were then subjected to fluorescent imaging using a Zeiss Axiovert 200 multi-channel fluorescence microscope (Carl Zeiss MicroImaging, Inc., Thornwood, NY, USA).

Results

Yeast strains heterozygous for *RPL33A* and *SDO1* deletions were obtained from Euroscarf or Research Genetics. The diploid strains were sporulated, tetrads dissected, and resulting haploid progeny grown on rich media. Compared with wild-type cells, cells harboring either deletion had a pronounced growth deficit (*data not shown*). To assess the effect of the *RPL33A* and *SDO1* deletions on the steady-state level of 60S subunits, extracts were prepared in low magnesium buffer in which polysomes and 80S monosomes dissociate completely into 40S and 60S ribosomal subunits. The ratio of 60S to 40S subunits was used to examine the selective effect of these mutations on 60S subunit levels beyond any overall reduction in ribosome synthesis linked to reduced growth rate. Figure 1 illustrates that both yeast models exhibit a reduction in the quantity of 60S subunits relative to 40S subunits when compared to wild-type cells. The relative reduction of 60S subunits in the two mutant strains differed by approximately 10% with the *ΔRPL33A* showing the greater overall reduction.

Pulse-chase analysis of pre-rRNA processing was used for a more detailed characterization of subunit maturation in the DBA and SDS disease models. The yeast pre-rRNA processing pathway is shown in Figure 2A. Relative to the wild-type strain, the *RPL33A* mutant showed a pronounced delay in the production of mature 25S rRNA such that by 10 min of chase the amount of radio-label in 25S rRNA relative to 18S rRNA was significantly less than the approximate 2:1 ratio observed in wild-type cells (Figure 2B top panel). This selective effect on 25S rRNA synthesis was accompanied by delayed maturation of several pre-rRNA precursors including 35S, 23S, and 27S pre-rRNA. The delayed maturation of 35S and 23S pre-rRNA was the result of an ill-defined feedback system in which early steps in pre-rRNA processing are slowed in mutants that affect the maturation of 60S subunits.[25] The delayed maturation of 27S pre-rRNA species, on the other hand, accounted for the selective effect of the *ΔRPL33A* mutant on the maturation of 60S subunits. The top panel of Figure 2B shows a 27S pre-rRNA doublet that persisted through the 10-min chase period. This doublet consisted of 27S A_2/A_3 species (upper band) and 27S B (lower band). The primary effect of the *RPL33A* deletion was a delay in maturation of 27S A_3/A_3 pre-rRNA as evidenced by the increased ratio of 27S A_2/A_3 to 27S B pre-rRNA observed by northern analysis (Figure 2C). The data from the *ΔSDO1* strain, on the other hand, revealed a more complex effect on 60S subunit maturation. As for the *ΔRPL33A* strain, there was a delay in 35S and 23S pre-rRNA processing, consistent with the feedback effect of a reduction in 60S subunits on early steps in pre-rRNA processing. The persistence of 35S and 23S pre-rRNA in the *ΔSDO1* strain indicates that cleavage steps A_0 and A_1 involved in the maturation of the 5' end of 18S rRNA may be more adversely affected when compared with the *ΔRPL33A* strain. Moreover, there was clearly a delay in 27S B pre-rRNA processing apparent by pulse-chase analysis in the *ΔSDO1* mutant relative to wild-type cells (Figure 2B, bottom panel); this delay could also be observed by northern analysis (Figure 2C). Surprisingly, however, the effect of this delay on the production of 25S rRNA did not appear to be as great as that observed in the *ΔRPL33A* strain since the ratio of 25S to 18S rRNA in this strain was still greater than one.

A more comprehensive analysis of the protein synthetic apparatus in the two disease models was made based

on polysome profiles. Polysome profiles from the *ΔRPL33A* strain showed a marked reduction in free 60S subunits relative to wild-type and the appearance of half-mer polysomes (Figure 3, middle panel). Half-mer polysomes are polysomes with stalled 48S initiation complexes and are a common characteristic of yeast strains with a deficit of 60S subunits.[26] The polysome profiles from the *ΔSDO1* strain also exhibited half-mer polysomes, but in contrast to the *ΔRPL33A* strain, there was a significant pool of free 60S subunits and a noteworthy decrease in mean polysome size (Figure 3, bottom panel). These data differ from previously reported polysome data from *SDO1* mutants when neither half-mer polysomes nor a free pool of 60S subunits was observed.[14] Both mutant strains show a peak to the left of the 40S peak which is absent in the wild-type strain. This peak was shown to contain 20S RNA, an endogenous virus-like particle induced by various forms of translational stress.[27]

To evaluate the intracellular distribution of 60S subunits in the two disease models, 60S subunits were tracked using a GFP-Rpl25 fusion protein. Several studies have shown that this protein is assembled into 60S subunits and can be used to monitor the distribution of such subunits within cells. In wild-type cells GFP fluorescence was distributed throughout nuclear and cytoplasmic regions but was reduced in intensity in the region corresponding to resident vacuoles (Figure 4, top panel). In *ΔRPL33A* cells cytoplasmic GFP fluorescence intensity was diminished, with discrete regions of enhanced GFP fluorescence that coincided with Nop1 and DAPI staining (Figure 4, middle

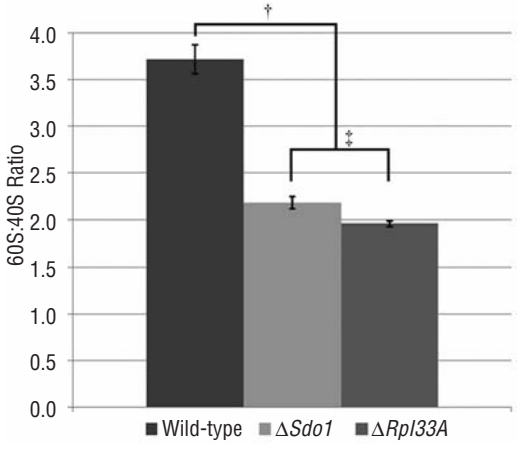

Figure 1. Yeast models of DBA and SDS both exhibit deficits in the relative amount of 60S to 40S ribosomal subunits. Extracts for subunit analysis were prepared as described for polysome isolation except magnesium was omitted from the buffers. Ribosomal subunits were resolved on 7-47% stepwise sucrose gradients via centrifugation. Gradients were broken down and the absorbance at 254 nm monitored using a gradient fractionator interfaced to a UA-6 absorbance detector. The bar graph denotes ratios of 60S to 40S in wild-type, *ΔSDO1*, and *ΔRPL33A* strains. Error bars corresponding to the standard error of the mean (SEM) are shown. Statistical significance was assessed by Student's *t* test. †Wild-type strain *versus* mutant strains (*P*<0.0001). ‡*ΔSDO1* strain *versus* *ΔRPL33A* strain (*P*<0.02).

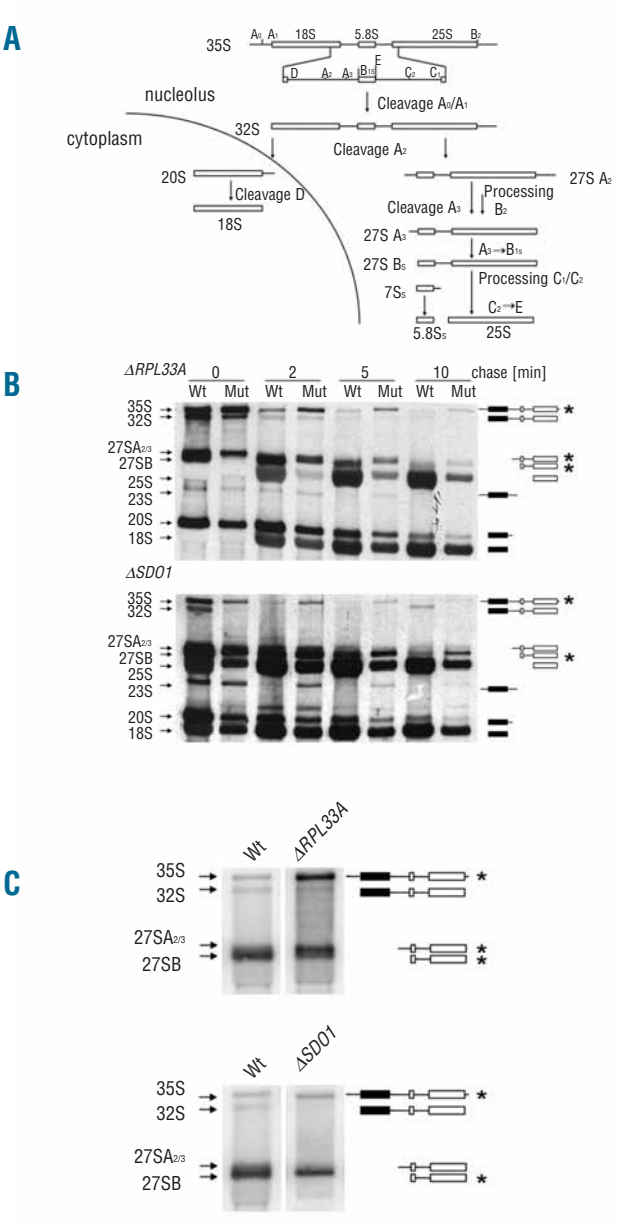

Figure 2. Yeast models of DBA and SDS display discrete pre-rRNA processing defects. (A) The major pre-rRNA processing pathway in *S. cerevisiae*. Mature rRNA species are represented by boxes. External and internal transcribed sequences are shown as thin lines. Numbered letters indicate processing sites. Horizontal arrows represent exonucleolytic cleavages; other cleavage steps are endonucleolytic. An alternative pathway which is not shown has cleavage at site A_2 preceding cleavages at sites A_0 and A_1 giving rise to 23S pre-rRNA. (B) Pulse-chase analysis of pre-rRNA processing in yeast models of DBA and SDS. Top panel, *ΔRPL33A* strain (Mut) and isogenic wild-type (Wt); bottom panel, *ΔSDO1* strain (Mut) and isogenic wild-type (Wt). Cells were pulse-labeled for 2 min with [methyl-^{3}H]-methionine and chased in the presence of 1 mg/mL methionine for the indicated times. Total RNA was prepared and fractionated as outlined in the Design and Methods section. Mature and pre-rRNA species are labeled to the left of each panel. Schematic diagrams to the right correlate to each of the pre-rRNA processing intermediates noted to the left. Species showing delayed processing relative to wild-type are marked with an asterisk. (C) Northern blot analysis of pre-rRNA processing in yeast models of DBA and SDS. Total RNA was prepared and fractionated as outlined in the Design and Methods section. A radiolabeled oligonucleotide probe that hybridized between the E and C_2 processing sites located within internal transcribed spacer 2 (ITS2) was used for northern analyses. Membranes were exposed to BioMax MS film at -80°C using a BioMax LE intensifying screen or were subjected to phosphorimage analysis.

panel). Rpl33, like many yeast ribosomal proteins, is encoded by duplicated genes that are nearly identical. Therefore, the cytoplasmic staining within these cells presumably results from the incorporation of Rpl33B into 60S subunits. The nucleolar localized GFP fluorescence observed in the *ΔRPL33A* strain likely represents the modest accumulation of immature 60S subunits as a consequence of delayed pre-rRNA processing at sites A_2 and A_3. The overall reduction in GFP-Rpl25 staining in the *ΔRPL33A* strain relative to wild-type indicates that these immature precursors are subject to enhanced decay. In contrast, *ΔSDO1* strains showed a pronounced accumulation of fluorescence in regions that broadly encompass Nop1 and DAPI staining and likely represent the retention of more fully matured 60S subunits in the nucleoplasm (Figure 4, bottom panel). Given the relative reduction of 60S subunits in the *ΔSDO1* strain observed from the subunit profiles in Figure 1, we believe a fraction of these more fully matured subunits accumulating in the absence of Sdo1 undergo degradation, albeit at a much slower rate than that observed for immature subunits in the *ΔRPL33A* strain. Collectively, these data indicate that the defect in 60S subunit maturation between the two disease models occurs at a later step in the *ΔSDO1* strain than in the *ΔRPL33A* strain, resulting in the accumulation of more fully matured precursors in the former relative to the latter.

Based on the emerging role for the 5S rRNA subcomplex in signaling abortive ribosome assembly to p53 activation in mammalian cells, we examined the fate of 5S rRNA in the yeast models of DBA and SDS. In wild-type cells, 5S rRNA was found in fractions corresponding to 60S subunits, 80S monosomes, and polysomes, with only a small fraction of extra-ribosomal 5S rRNA found near the top of the gradient (Figure 5). In *ΔRPL33A* extracts there was a dramatic increase in the amount of extra-ribosomal 5S rRNA found near the top of the gradient (~41% of the total 5S RNA relative to ~11% for wild-type extracts), while in other regions of the gradient the amount of 5S rRNA was reduced. This latter observation is consistent with the absorbance tracings of the gradient profiles which showed an almost complete loss of free 60S subunits and a lower level of polysomes including half-mer polysomes, relative to wild-type (Figure 3). As for the *ΔRPL33A* strain, extracts from the *ΔSDO1* strain showed a significant reduction in the amount of 5S rRNA in the polysome region of the gradient compared to wild-type. In contrast to extracts of the *ΔRPL33A* strain, *ΔSDO1* extracts showed a substantial peak of 5S rRNA in the 60S region with this peak being comparable to that of the wild-type strain. The ratio of 5S to 5.8S rRNA in this peak was similar to that found in 80S and polysome regions indicating that this free pool of 60S subunits contains stoichiometric amounts of these two mature rRNA species. The increase in 5S rRNA in the 60S region in *ΔSDO1* extracts was associated with a smaller amount of extra-ribosomal 5S rRNA (~27% of total 5S RNA) found near the top of the gradient when compared with the *ΔRPL33A* strain. Thus, the two disease models differ dramatically in their effect on subunit assembly and stability including differences in the fate of 5S rRNA as a consequence of these distinct effects on 60S subunit maturation.

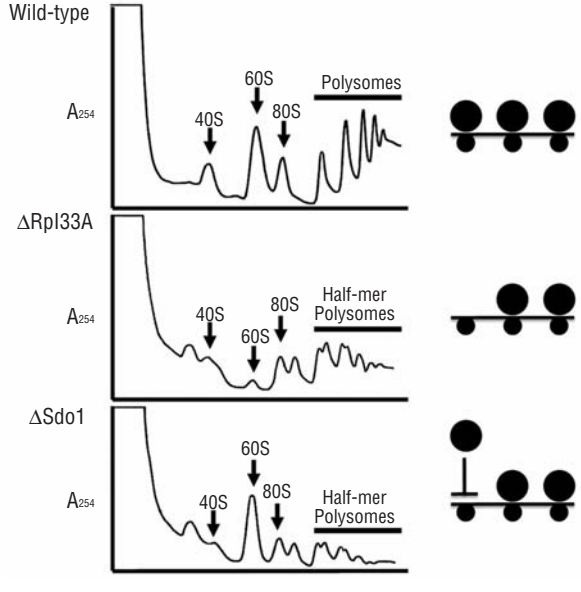

Figure 3. Polysome profiles from yeast models of DBA and SDS differ in the amount of free 60S subunits. Top panel, wild-type; middle panel, *ΔRPL33A*; bottom panel, *ΔSDO1*. Cell extracts were prepared and fractionated as outlined in the *Design and Methods* section. Subunit peaks were identified by analyzing the rRNA species co-sedimenting with each peak (*data not shown*). The left hand side of each panel represents the top of the sucrose gradients. The schematic diagrams to the right of the mutant profiles indicate that half-mer polysomes arise as a consequence of a 60S subunit deficit in the *ΔRPL33A* whereas in the *ΔSDO1* strain 60S subunits are present but unable to engage in translation. Polysome analysis was performed in triplicate for each strain.

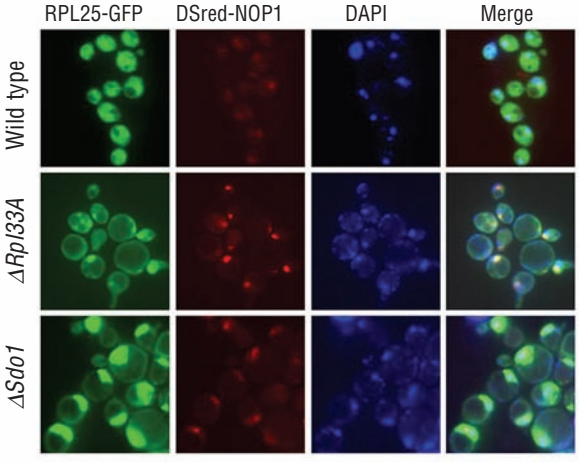

Figure 4. Nuclear retention of pre-60S subunits in the yeast SDS model. Live cell fluorescence images corresponding to wild-type (top row), *ΔRPL33A* (middle row), and *ΔSDO1* (bottom row) strains are shown. Wild-type and mutant strains were transformed with Rpl25-GFP (a component of 60S ribosomal subunits) and Nop1-DSRED (nucleolar protein). Left column, Rpl25-GFP fluorescence; middle left column, Nop1-RFP; middle right column, DAPI stain; right column, merge of all three images. Images depicted were chosen to be accurate representations of a collection of fluorescence studies performed in triplicate.

Discussion

The recent finding that DBA can be caused by mutations in genes encoding large subunit ribosomal proteins has a number of implications.[8,9] This observation now suggests that any of the approximately 60 genes encoding large subunit ribosomal proteins could be mutated in DBA patients whose genetic lesion is unknown. Furthermore, this observation continues to support the notion that DBA is caused by mutations in genes encoding structural components of the ribosome and that either subunit can be affected. For the purposes of the present study, the finding that 60S subunit ribosomal proteins are affected in DBA allowed for a more direct comparison of the underlying molecular bases for DBA and SDS, as the target in SDS also appears to be the 60S ribosomal subunit.[13,14]

The yeast models of DBA and SDS examined here are both associated with a selective reduction in the amount of 60S ribosomal subunits. This reduction was more severe in *ΔRPL33A* extracts relative to *ΔSDO1* extracts when total subunit analysis was performed. In both cases, the reduced amount of 60S subunits was associated with the appearance of half-mer polysomes upon polysome analysis. Half-mer polysomes are polysomes with stalled 48S initiation complexes generally linked to defects in 60S subunit synthesis.[26] In this case, subunit joining is delayed in forming 80S initiation complexes leaving 48S initiation complexes stalled at the initiation codon. The reduction in 60S subunits in the *ΔRPL33A* strain occurred at the level of 27S A_2/A_3 pre-rRNA processing, which resulted in delayed production of 27S B pre-rRNA and reduced amounts of mature 5.8S and 25S rRNA. A related defect in the production of 60S ribosomal subunits has recently been demonstrated for a yeast strain harboring a missense mutation in *RPL33A*.[28]

In the yeast model of SDS, half-mer polysomes were observed in cells that still had a substantial pool of free 60S ribosomal subunits. These results differ dramatically from those in a previous study of an *ΔSDO1* deletion strain in which half-mer polysomes were not observed despite an apparent reduction in the amount of 60S subunits.[14] These previous findings are difficult to explain since numerous studies have shown that a reduction in 60S subunits gives rise to half-mer polysomes.[25] Our data reveal that there is also a delay in pre-rRNA processing in the *ΔSDO1* strain, but that this delay occurs at the level of 27S B pre-rRNA, downstream of the effect observed in cells depleted of Rpl33A. This delay is also associated with the retention of a significant fraction of 60S subunits within the nuclei of *ΔSDO1* cells. Thus, the effect of the SDO1 mutation on the amount of 60S subunits available for translation in the cytoplasm represents a combined effect of both delayed pre-rRNA processing and nuclear retention. This interpretation is in general agreement with conclusions reached previously on the role of Sdo1 in recycling Tif6 from the cytoplasm to the nucleus where it is involved in 60S subunit maturation, but differs significantly from the previous report in the supporting data.[14]

Comparing the two disease models we have shown that they differ in their effect on the maturation of 60S subunits (Figure 6). Both 35S pre-rRNA and 5S rRNA are found in 90S pre-ribosomal particles assembled early in the ribosome maturation pathway.[29] The maturation defect in the DBA model occurs earlier in the pathway and is accompanied by the rapid degradation of incompletely assembled precursors. In contrast, the maturation defect in the SDS model is associated with delayed export, and accumulation of 60S-like particles in the nucleoplasm. The differences in the mechanism by which ribosome maturation is disrupted in these yeast models of DBA and SDS could, therefore, form the basis for different types of nucleolar/nuclear stress signaling and be responsible for the distinct clinical presentations of the two diseases in humans.

Accumulating data suggest that nucleolar stress signaling linked to abortive ribosome assembly plays an important role in the pathophysiology of DBA. Studies in zebra fish[16] and mouse[17] models of DBA suggest that p53 stabilization and activation promoted by nucleolar stress signaling is critical for phenotypes associated with ribosomal protein haploinsufficiency. While many potential mechanisms can explain p53 activation and stabilization under

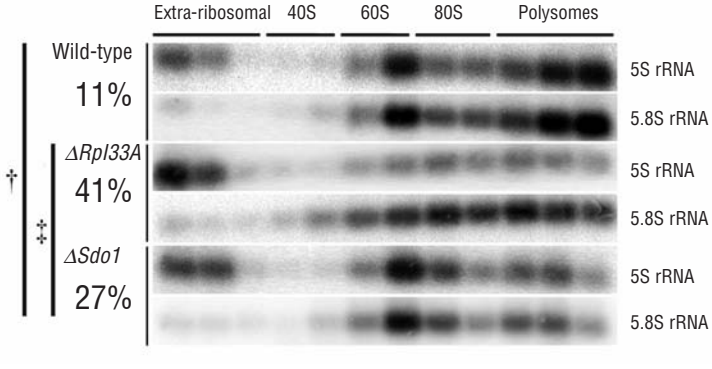

Figure 5. The yeast DBA model has an increased amount of extra-ribosomal 5S rRNA. Each row depicts a total of 12 precipated RNA fractions spanning the 7-47% stepwise sucrose density gradients of resolved polysome extracts corresponding to wild-type (top two rows), *ΔRPL33A* (middle two rows), and *ΔSDO1* (bottom two rows) yeast strains. RNA samples were immobilized to nylon membranes via UV crosslinking and incubated with radiolabeled oligonucleotide probes to either 5S or 5.8S rRNA (labels are shown to the right). The percentage of extra-ribosomal 5S rRNA for each yeast strain is depicted to the left of each northern blot and is expressed as a mean. Student's t test was used to test for statistical significance. The percentage of extra-ribosomal 5S rRNA is representative of the ratio of 5S rRNA at the top of the gradient divided by the total 5S rRNA within a gradient. †Wild-type versus mutant strains ($P<0.004$); ‡*ΔRPL33A versus ΔSDO1* ($P<0.01$).

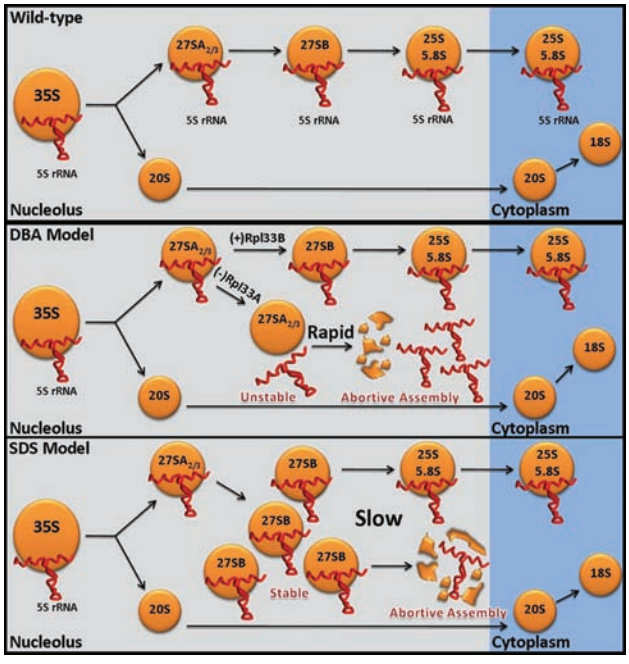

Figure 6. Ribosomal subunit maturation in *ΔRPL33A* and *ΔSDO1* strains. Diagrammatic representations of ribosomal subunit maturation in wild-type (top panel), *ΔRPL33A* (middle panel), and *ΔSDO1* (bottom panel) yeast strains are shown and are described in detail in the text. Orange circles represent either the 90S pre-ribosomal particle or 40S or 60S ribosomal subunit precursors. Fractured circles represent precursor degradation. Relevant steps in pre-rRNA processing are labeled. 5S rRNA is labeled and shown in red.

conditions of stress, recent studies have identified mechanisms more specific to nucleolar stress induced by abortive ribosome assembly.[19,30] Three large subunit ribosomal proteins have been shown to bind to MDM2 and promote p53 stabilization and activation. Two of these proteins, Rpl5 and Rpl11, have been shown to bind synergistically with MDM2, most likely mediated through their interaction with 5S rRNA.[23] We were, therefore, interested in following the fate of 5S rRNA in our yeast models of DBA and SDS in an effort to determine whether the maturation defects outlined above influenced 5S rRNA assembly.

Intriguingly, both disease models showed an increase in extra-ribosomal 5S rRNA relative to wild-type. 5S rRNA is distinct from the other three mature rRNA species in that 5S rRNA is transcribed by RNA polymerase III, distinct from the 35S polycistronic precursor transcribed by RNA polymerase I, which gives rise to 25S, 18S, and 5.8S rRNA.[25] Moreover, 5S rRNA forms a subcomplex with Rpl5, Rpl11 and specific assembly factors within 60S subunit precursors.[29] Whether this subcomplex forms prior to joining 60S subunit precursors or after individual components of the subcomplexes have been incorporated into maturing subunits has not yet been determined.[29] According to the data reported here, the extra-ribosomal pool of 5S rRNA in wild-type cells accounts for only about 10% of the total 5S rRNA on sucrose gradients. This extra-ribosomal pool increases to approximately 40% of total 5S rRNA in *ΔRPL33A* extracts (Figure 5). This increase could be a reflection of the inability of assembly intermediates lacking Rpl33A to stably incorporate components of the 5S rRNA subcomplex into 60S subunit precursors. The extent to which components of the 5S subcomplex depend on Rpl33A for incorporation into assembling 60S subunits is currently unknown.[31] The observation that depletion of Rpl33A blocks pre-rRNA processing upstream of 27S B pre-rRNA, which accumulates in cells depleted of components of the 5S subcomplex,[29,32] is consistent with Rpl33A acting earlier in the pathway than components of the 5S subcomplex. We cannot, however, rule out the possibility that the increased extra-ribosomal 5S rRNA observed in cells depleted of Rpl33A results from the release of bound 5S subcomplex from abortive assembly intermediates targeted for degradation.

In contrast to the data obtained with the *ΔRPL33A* strain, our data show that 5S rRNA co-sediments with the large pool of free 60S subunits observed in *ΔSDO1* cells. Our fluorescence data indicate that a considerable fraction of this pool of free 60S subunits in *ΔSDO1* cells is retained within the nucleus. This pool of free 60S subunits likely represents pre-60S subunit precursors containing either 27S B pre-rRNA or pre-60S subunit precursors even further along the maturation pathway containing mature 25S and 5.8S rRNA.[33] The ratio of 5S to 5.8S rRNA in the free 60S subunit peak is similar to the ratio of 5S to 5.8S rRNA in functional 60S subunits found in the polysome fractions, indicating that 5S rRNA has been incorporated into the nuclear-retained subunits in *ΔSDO1* cells. The decreased amount of total 60S subunits in these cells suggests that this pool of pre-60S subunits may be turned over at a higher rate than mature 60S subunits that reach the cytoplasm. It is an interesting possibility that the increased amounts of extra-ribosomal 5S rRNA in *ΔSDO1* strains may be a consequence of the release of the 5S subcomplex from pre-60S particles targeted for degradation.

Some caveats should be considered in regarding an integral role for components of the 5S rRNA subcomplex in signaling mechanisms that link abortive ribosome assembly to p53 stabilization and activation as a molecular basis for DBA. First, it is the general view that the assembly of 60S ribosomal subunits is largely independent of the assembly of 40S subunits, suggesting that haploinsufficiency for a small subunit ribosomal protein should not interfere with steps in 60S subunit assembly. However, recent results from mammalian systems revealed that disruption of 40S subunit maturation resulted in an up-regulation of translation of Rpl11.[34] This up-regulation presumably results in Rpl11 being synthesized in excess of that needed for 60S subunit assembly which, in turn, interacts with MDM2 leading to p53 activation. These studies did not however, address whether Rpl11 functioned in concert with other components of the 5S rRNA subcomplex in this signaling pathway. A second caveat with regard to a critical role for Rpl5 and Rpl11 signaling in the pathophysiology of DBA is the finding that *RPL5* and *RPL11* have both been identified as genes mutated in DBA.[9] Here it is difficult to envision how proteins that presumably limit ribosome assembly in an affected patient could also have an important role in signaling via an interaction with MDM2. The observation that patients with mutations in *RPL5* have distinct clinical phenotypes suggests that alter-

native signaling pathways may operate in patients with mutations in *RPL5* or *RPL11*.[9]

Despite these caveats, we feel our yeast data support a potential role for the 5S ribonucleoprotein subcomplex in the pathogenesis of DBA. Moreover, the differences in the mechanisms by which 60S subunit maturation is affected in the DBA and SDS models and their influence on the 5S subcomplex suggest that this subcomplex may also be important in explaining how defects in the maturation of 60S ribosomal subunits can give rise to distinct clinical phenotypes.

Authorship and Disclosures

SRE was the principal investigator and takes primary responsibility for all aspects of the paper. JBM performed many of the experiments and participated in data analysis and writing the manuscript. JEF, RJA, and JML contributed to experimental design, data analysis, and writing the manuscript.

SRE is employed to the Trover Scholars Program.

The other authors reported no potential conflicts of interest.

References

1. Liu JM, Ellis SR. Ribosomes and marrow failure: coincidental association or molecular paradigm? Blood. 2006;107(12):4583-8.
2. Hall GW, Dale P, Dodge JA. Shwachman-Diamond syndrome: UK perspective. Arch Dis Child. 2006;91(6):521-4.
3. Freedman MH. Diamond-Blackfan anaemia. Baillieres Best Pract Res Clin Haematol. 2000;13(3):391-406.
4. Lipton JM, Atsidaftos E, Zyskind I, Vlachos A. Improving clinical care and elucidating the pathophysiology of Diamond Blackfan anemia: an update from the Diamond Blackfan Anemia Registry. Pediatr Blood Cancer. 2006;46(5):558-64.
5. Gazda HT, Grabowska A, Merida-Long LB, Latawiec E, Schneider HE, Lipton JM, et al. Ribosomal protein S24 gene is mutated in Diamond-Blackfan anemia. Am J Hum Genet. 2006;79(6):1110-8.
6. Draptchinskaia N, Gustavsson P, Andersson B, Pettersson M, Willig TN, Dianzani I, et al. The gene encoding ribosomal protein S19 is mutated in Diamond-Blackfan anaemia. Nat Genet. 1999;21(2): 169-75.
7. Cmejla R, Cmejlova J, Handrkova H, Petrak J, Pospisilova D. Ribosomal protein S17 gene (RPS17) is mutated in Diamond-Blackfan anemia. Hum Mutat. 2007;28(12): 1178-82.
8. Farrar JE, Nater M, Caywood E, McDevitt MA, Kowalski J, Takemoto CM, et al. Abnormalities of the large ribosomal subunit protein, Rpl35A, in Diamond-Blackfan anemia. Blood. 2008;112(5):1582-92.
9. Gazda HT, Sheen MR, Vlachos A, Choesmel V, O'Donohue MF, Schneider H, et al. Ribosomal protein L5 and L11 mutations are associated with cleft palate and abnormal thumbs in Diamond-Blackfan anemia patients. Am J Hum Genet. 2008; 83(6):769-80.
10. Flygare J, Aspesi A, Bailey JC, Miyake K, Caffrey JM, Karlsson S, et al. Human RPS19, the gene mutated in Diamond-Blackfan anemia, encodes a ribosomal protein required for the maturation of 40S ribosomal subunits. Blood. 2007;109(3): 980-6.
11. Choesmel V, Bacqueville D, Rouquette J, Noaillac-Depeyre J, Fribourg S, Cretien A, et al. Impaired ribosome biogenesis in Diamond-Blackfan anemia. Blood. 2007; 109(3):1275-83.
12. Idol RA, Robledo S, Du HY, Crimmins DL, Wilson DB, Ladenson JH, et al. Cells depleted for RPS19, a protein associated with Diamond Blackfan anemia, show defects in 18S ribosomal RNA synthesis and small ribosomal subunit production. Blood Cells Mol Dis. 2007;39(1):35-43.
13. Ganapathi KA, Austin KM, Lee CS, Dias A, Malsch MM, Reed R, et al. The human Shwachman-Diamond syndrome protein, SBDS, associates with ribosomal RNA. Blood. 2007;110(5):1458-65.
14. Menne TF, Goyenechea B, Sanchez-Puig N, Wong CC, Tonkin LM, Ancliff PJ, et al. The Shwachman-Bodian-Diamond syndrome protein mediates translational activation of ribosomes in yeast. Nat Genet. 2007;39(4): 486-95.
15. Uechi T, Nakajima Y, Chakraborty A, Torihara H, Higa S, Kenmochi N. Deficiency of ribosomal protein S19 during early embryogenesis leads to reduction of erythrocytes in a zebrafish model of Diamond-Blackfan anemia. Hum Mol Genet. 2008;17(20):3204-11.
16. Danilova N, Sakamoto KM, Lin S. Ribosomal protein S19 deficiency in zebrafish leads to developmental abnormalities and defective erythropoiesis through activation of p53 protein family. Blood. 2008;112(13):5228-37.
17. McGowan KA, Li JZ, Park CY, Beaudry V, Tabor HK, Sabnis AJ, et al. Ribosomal mutations cause p53-mediated dark skin and pleiotropic effects. Nat Genet. 2008; 40(8):963-70.
18. Pestov DG, Strezoska Z, Lau LF. Evidence of p53-dependent cross-talk between ribosome biogenesis and the cell cycle: effects of nucleolar protein Bop1 on G(1)/S transition. Mol Cell Biol. 2001;21(13):4246-55.
19. Lindstrom MS, Deisenroth C, Zhang Y. Putting a finger on growth surveillance: insight into MDM2 zinc finger-ribosomal protein interactions. Cell Cycle. 2007;6(4): 434-7.
20. Gjerset RA. DNA damage, p14ARF, nucleophosmin (NPM/B23), and cancer. J Mol Histol. 2006;37(5-7):239-51.
21. Maggi LB Jr, Kuchenruether M, Dadey DY, Schwope RM, Grisendi S, Townsend RR, et al. Nucleophosmin serves as a rate-limiting nuclear export chaperone for the mammalian ribosome. Mol Cell Biol. 2008; 28(23):7050-65.
22. Boocock GR, Morrison JA, Popovic M, Richards N, Ellis L, Durie PR, et al. Mutations in SBDS are associated with Shwachman-Diamond syndrome. Nat Genet. 2003;33(1):97-101.
23. Horn HF, Vousden KH. Cooperation between the ribosomal proteins L5 and L11 in the p53 pathway. Oncogene. 2008; 27(44):5774-84.
24. Leger-Silvestre I, Caffrey JM, Dawaliby R, Alvarez-Arias DA, Gas N, Bertolone SJ, et al. Specific role for yeast homologs of the Diamond Blackfan anemia-associated Rps19 Protein in ribosome synthesis. J Biol Chem. 2005;280(46):38177-85.
25. Venema J, Tollervey D. Ribosome synthesis in Saccharomyces cerevisiae. Annu Rev Genet. 1999;33:261-311.
26. Rotenberg MO, Moritz M, Woolford JL Jr. Depletion of Saccharomyces cerevisiae ribosomal protein L16 causes a decrease in 60S ribosomal subunits and formation of half-mer polyribosomes. Genes Dev. 1988; 2(2):160-72.
27. Wickner RB. Double-stranded RNA viruses of Saccharomyces cerevisiae. Microbiol Rev. 1996;60(1):250-65.
28. Martin-Marcos P, Hinnebusch AG, Tamame M. Ribosomal protein L33 is required for ribosome biogenesis, subunit joining, and repression of GCN4 translation. Mol Cell Biol. 2007;27(17):5968-85.
29. Zhang J, Harnpicharnchai P, Jakovljevic J, Tang L, Guo Y, Oeffinger M, et al. Assembly factors Rpf2 and Rrs1 recruit 5S rRNA and ribosomal proteins rpL5 and rpL11 into nascent ribosomes. Genes Dev. 2007;21(20):2580-92.
30. Sun XX, Dai MS, Lu H. 5-fluorouracil activation of p53 involves an MDM2-ribosomal protein interaction. J Biol Chem. 2007; 282(11):8052-9.
31. Nissan TA, Bassler J, Petfalski E, Tollervey D, Hurt E. 60S pre-ribosome formation viewed from assembly in the nucleolus until export to the cytoplasm. EMBO J. 2002;21(20):5539-47.
32. Dechampesme AM, Koroleva O, Leger-Silvestre I, Gas N, Camier S. Assembly of 5S ribosomal RNA is required at a specific step of the pre-rRNA processing pathway. J Cell Biol. 1999;145(7):1369-80.
33. Harnpicharnchai P, Jakovljevic J, Horsey E, Miles T, Roman J, Rout M, et al. Composition and functional characterization of yeast 66S ribosome assembly intermediates. Mol Cell. 2001;8(3):505-15.
34. Fumagalli S, Di Cara A, Neb-Gulati A, Natt F, Schwemberger S, Hall J, et al. Absence of nucleolar disruption after impairment of 40S ribosome biogenesis reveals an rpL11-translation-dependent mechanism of p53 induction. Nat Cell Biol. 2009;11(4):501-8.